

# Frequency and temperature dependence dielectric study of strontium modified Barium Zirconium Titanate ceramics obtained by mechanochemical synthesis

T. Badapanda · S. Sarangi · S. Parida ·  
B. Behera · B. Ojha · S. Anwar

Received: 5 December 2014 / Accepted: 31 January 2015 / Published online: 11 February 2015  
© Springer Science+Business Media New York 2015

**Abstract** A detailed investigation of the crystal structure and electrical properties of  $\text{Ba}_{1-x}\text{Sr}_x\text{Zr}_{0.05}\text{Ti}_{0.95}\text{O}_3$  ( $x = 0.1, 0.2, 0.3$  and  $0.5$ ) ceramics prepared using high energy ball milling is presented in this manuscript. The X-ray diffraction patterns confirmed the single phase formation of the examined compounds. The substitution of  $\text{Sr}^{2+}$  drove the crystal symmetry of the system from tetragonal to cubic at  $x = 0.3$ . The structural conformation was also carried out employing the Rietveld refinement analysis. The microstructural study was developed through the scanning electron microscopy, which showed a decrement in the grain size with Sr doping. Using the impedance spectroscopic technique, the electrical microstructure of the system was presented and the overall electrical properties indicated the presence of grains separated by grain boundaries and is explained in terms of the bricklayer model. Negative temperature coefficient of resistance behavior was observed in all compositions. The activation energy estimated from impedance, modulus and conductivity formalism confirmed that the oxygen vacancies play an important role in the conduction mechanism.

## 1 Introduction

$\text{BaTiO}_3$  (BT) based perovskite materials have been extensively studied owing to their remarkable dielectric, ferroelectric, piezoelectric and pyroelectric properties throughout the last decades [1–4]. They are also an important electroceramic due to their applications in multilayer ceramic capacitor (MLCC), positive temperature coefficient of resistance (PTCR) Thermistors, piezoelectric sensors, transducers and electro-optic devices [5–9]. Barium titanate has a special place in the perovskite group of compounds because it forms a solid solution with other perovskites with a wide range of compositions which leads to various applications. For many years, A- and B-site dopants have been used to modify the electrical properties of  $\text{BaTiO}_3$ . It is well known that semiconducting barium titanate shows the PTCR (positive temperature coefficient of resistivity) effect near its Curie temperature. To lower the Curie temperature and to improve the temperature stability  $\text{Zr}^{4+}$  is substituted for  $\text{Ti}^{4+}$  as  $\text{Zr}^{4+}$  is more stable than  $\text{Ti}^{4+}$ . It is also reported in the literature that the addition of small amounts of  $\text{ZrO}_2$  (<5 mol%) to  $\text{BaTiO}_3$  raises the band gap of  $\text{Ba}(\text{Ti}_{1-x}\text{Zr}_x)\text{O}_3$  solid solution (from 2.89 to 3.01 eV at 2 % Zr) and thus lowers electrical conductivities [10]. Moreover, the reduction enthalpy is also significantly raised by the presence of Zr (from 5.6 eV for  $\text{BaTiO}_3$  to 7.3 eV at 2 % Zr), which consequently suppresses the reduction process, leading to decrease in the formation of oxygen vacancies with lower electrical conductivities [11]. Again, in order to lower the grain internal resistivity  $\text{SrTiO}_3$  is widely used as basic composition which will shift the capacitance dispersion to higher frequency, and promote the stability of bias dependence.  $\text{Sr}^{2+}$  (0.144 nm) and  $\text{Zr}^{4+}$  (0.072 nm) have similar ionic radii but  $\text{Ba}^{2+}$  (0.161 nm) and  $\text{Ti}^{4+}$  (0.061 nm). Thus,  $\text{BaTiO}_3$

---

T. Badapanda (✉) · S. Parida  
Department of Physics, C.V. Raman College of Engineering,  
Bhubaneswar 752054, Odisha, India  
e-mail: badapanda.tanmaya@gmail.com

S. Sarangi · B. Behera  
School of Physics, Sambalpur University, Jyoti Vihar,  
Sambalpur 768019, Odisha, India

B. Ojha  
Department of Physics, College of Engineering & Technology,  
Ghatikia, Bhubaneswar 751003, Odisha, India

S. Anwar  
Colloids & Materials Chemistry, Institute of Minerals and  
Materials Technology, Bhubaneswar 751013, Odisha, India

easily forms complete solid solutions with  $\text{SrTiO}_3$  and  $\text{BaZrO}_3$  [12, 13].

In order to know the overall electrical properties of any material, understanding of its microstructure, which mainly comprises grains and grain boundaries, is really essential. To distinguish between transport characteristics of grains and grain boundaries, impedance spectroscopy is a useful technique. This technique is capable to resolve the contribution of different phases such as grain interior, grain boundaries, and the electrode-sample contacts; furthermore, by employing impedance spectroscopy it is possible to determine the presence of any impurity phase in the sample regarding grain boundaries, which can act as carrier traps and form the barrier layer for charge transport. Emphasis has been put on understanding electrical behavior on the effect co doping  $\text{Sr}^{2+}$  and  $\text{Zr}^{4+}$  in  $\text{BaTiO}_3$  perovskite using impedance spectroscopy study.

## 2 Experimental

Strontium doped Barium Zirconium Titanate (BSZT) with general formula  $\text{Ba}_{1-x}\text{Sr}_x\text{Zr}_{0.05}\text{Ti}_{0.95}\text{O}_3$  ( $x = 0.0, 0.1, 0.2, 0.3$  and  $0.5$ ) ceramic powders were prepared by a combination of solid state reaction and high energy ball milling technique. The ball to powder ratio (BPR) was maintained at 20:1 by weight.  $\text{BaCO}_3$  (99.9 %),  $\text{SrCO}_3$  (99.9 %),  $\text{ZrO}_2$  (99.8 %) and  $\text{TiO}_2$  (99.95 %) were used as starting materials and stoichiometric amounts of these materials were weighed. The high energy ball milling of these weighed powders were carried out in a Fritsch planetary. For proper mixing of the weighed powders, the powders were mixed in tungsten carbide balls (10 mm diameter) with toluene as

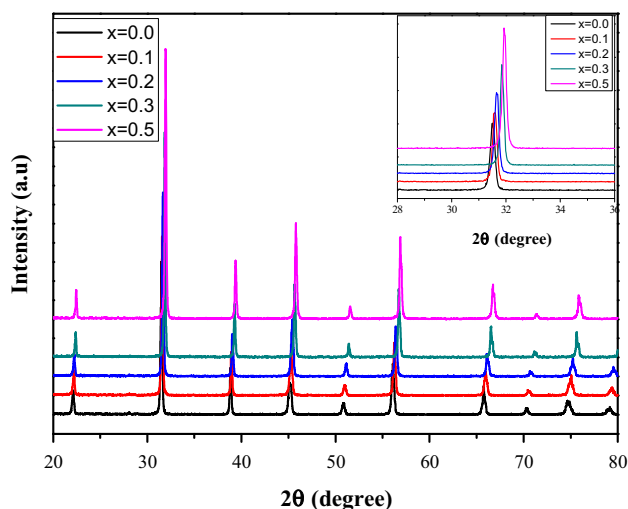


**Fig. 1** XRD patterns of  $\text{Ba}_{1-x}\text{Sr}_x\text{Zr}_{0.05}\text{Ti}_{0.95}\text{O}_3$  ceramic calcined powder at  $1,100\text{ }^\circ\text{C}$  for 4 h (insert shows reduced XRD patterns of BSZT ceramics)

milling media for 5 h at 300 RPM. The milled powders were treated at  $1,100\text{ }^\circ\text{C}$  for 4 h in a programmable furnace.

The synthesized powder was structurally characterized by X-ray diffraction (XRD) using a Philips diffractometer model PW-1830 with  $\text{Cu-K}\alpha$  ( $\lambda = 1.5418\text{ \AA}$ ) radiation in a wide range of  $2\theta$  ( $20 \leq 2\theta \leq 70$ ) at a scanning rate of 2 degree per min. In order to measure the electrical properties of BSZT ceramics, the disc was pressed uniaxially at 200 MPa with 2 wt % polyvinyl alcohol added as a binder. Afterwards, this discs were sintered at  $1,200\text{ }^\circ\text{C}$  for 4 h. Silver contacts were deposited on the opposite disc faces and heated at  $700\text{ }^\circ\text{C}$  for 15 min. The frequency (1 Hz–1 MHz) and temperature ( $30\text{--}500\text{ }^\circ\text{C}$ ) dependent dielectric measurements were carried out using a N4L-NumetriQ (model PSM1735) connected to a computer.

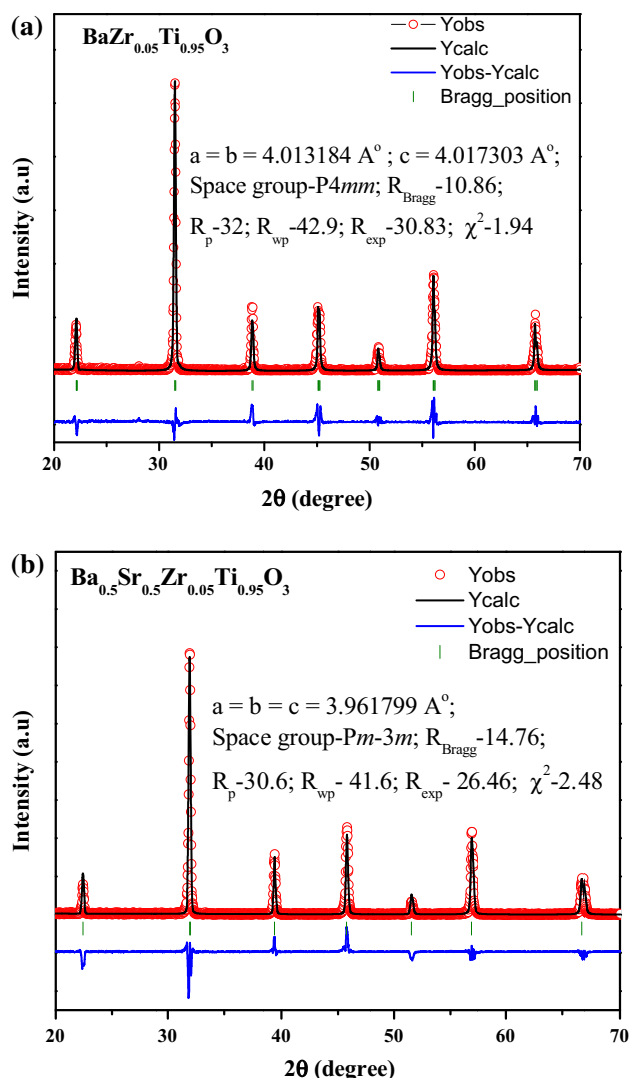


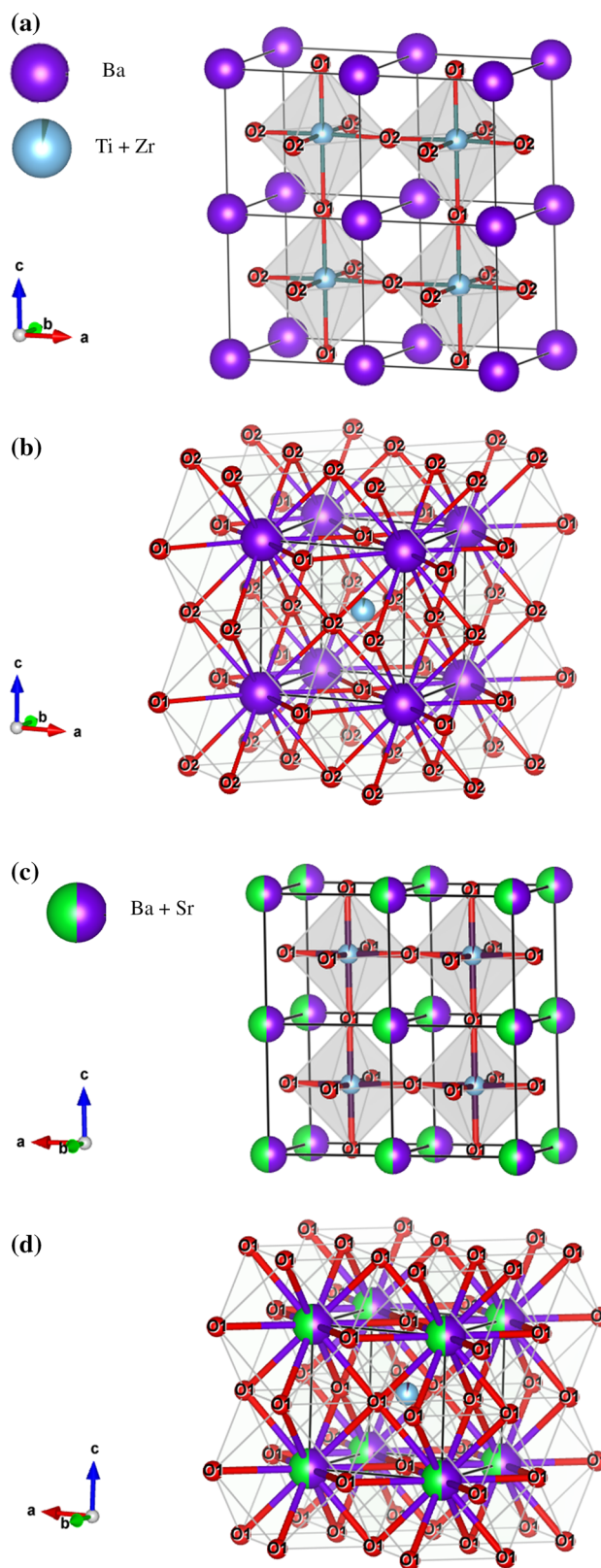
**Fig. 2** Rietveld Refinement of  $\text{Ba}_{1-x}\text{Sr}_x\text{Zr}_{0.05}\text{Ti}_{0.95}\text{O}_3$  ceramic **a**  $x = 0.0$  and **b**  $x = 0.5$

**Fig. 3** Supercells ( $2 \times 2 \times 2$ ) for the  $Ba_{1-x}Sr_xZr_{0.05}Ti_{0.95}O_3$  ceramics with **a**  $x = 0$  and **c**  $x = 0.5$  illustrating the [TiO6], [ZrO6],[BaO12]/[SrO12] clusters, Barium (Ba) atoms and Strontium (Sr) atoms are coordinated to twelve O atoms [BaO12] clusters **b**  $x = 0.0$  and **d**  $x = 0.5$

### 3 Result and discussion

#### 3.1 Structural studies

Figure 1 displays the room temperature X-ray diffraction spectra of  $Ba_{1-x}Sr_xZr_{0.05}Ti_{0.95}O_3$  system for  $x = 0.0, 0.1, 0.2, 0.3,$  and  $0.5$ . It clearly indicates the single phase formation of the examined compounds and confirms the complete solid solubility of  $Sr^{2+}$  up to  $x = 0.5$  in BZT. The crystal symmetry of the system remains in tetragonal up to  $x = 0.3$  and with further increase in  $Sr^{2+}$  the structure changes to cubic. A close observation of the X-ray diffraction data indicates a shift in diffraction peaks toward higher  $2\theta$  values (insert of Fig. 1). This is translated as the reduction of the lattice parameter with an increase in the  $Sr^{2+}$  content. The reduction in the lattice parameter can be explained because of the low ionic radius  $Sr^{2+}$  ion ( $1.44 \text{ \AA}$ ) substituting the higher ionic radius  $Ba^{2+}$  ion ( $1.61 \text{ \AA}$ ). Figure 2a, b illustrate the structural refinement using the Rietveld method confirming that the XRD patterns of BSZT ceramic with different compositions: [(a)  $x = 0$ ; (b)  $x = 0.5$ ]; are monophasic with a perovskite-type tetragonal structure and cubic structure, respectively. Rietveld refinements performed using the Full prof software involved Rietveld texture and stress analysis. The optimized parameters were scale factor, background with exponential shift, exponential thermal shift, polynomial coefficients, basic phase, microstructure, crystal structure, structure factor extractor, shift lattice constants, profile half-width parameters ( $u, v, w$ ), lattice parameters ( $a, b, c$ ), Wyckoff, site occupancy, and occupancy. These parameters were used to obtain a structural refinement with better quality and reliability. The fitting parameters ( $R_p, R_{exp}, R_{wp}, \chi^2,$  and GoF) indicate good agreement between refined and observed XRD patterns. Figure 3a,c shows the schematic representation of crystalline super cells for BSZT ceramics with (a)  $x = 0$ , and (b)  $x = 0.5$ . Lattice parameters and atomic positions obtained from Rietveld refinements were used to model these supercells through the Visualization for Electronic and Structural Analysis (VESTA) program, version 3.1.7, for Windows. Figure 3a,c illustrates super cells ( $2 \times 2 \times 2$ ) for the BSZT ceramics with (a)  $x = 0$ ; perovskite-type tetragonal structure of a space group of ( $P4mm$ ) and (c)  $x = 0.5$ , perovskite-type cubic structure of a space group of ( $Pm3m$ ) respectively. In these supercells, zirconium (Zr) and titanium (Ti) atoms are coordinated to six oxygen (O) atoms which form octahedral [TiO6]/[ZrO6] clusters. Moreover,



Barium (Ba) atoms and Strontium (Sr) atoms are coordinated to twelve O atoms which form cuboctahedral [BaO12] clusters (Fig. 3b,d).

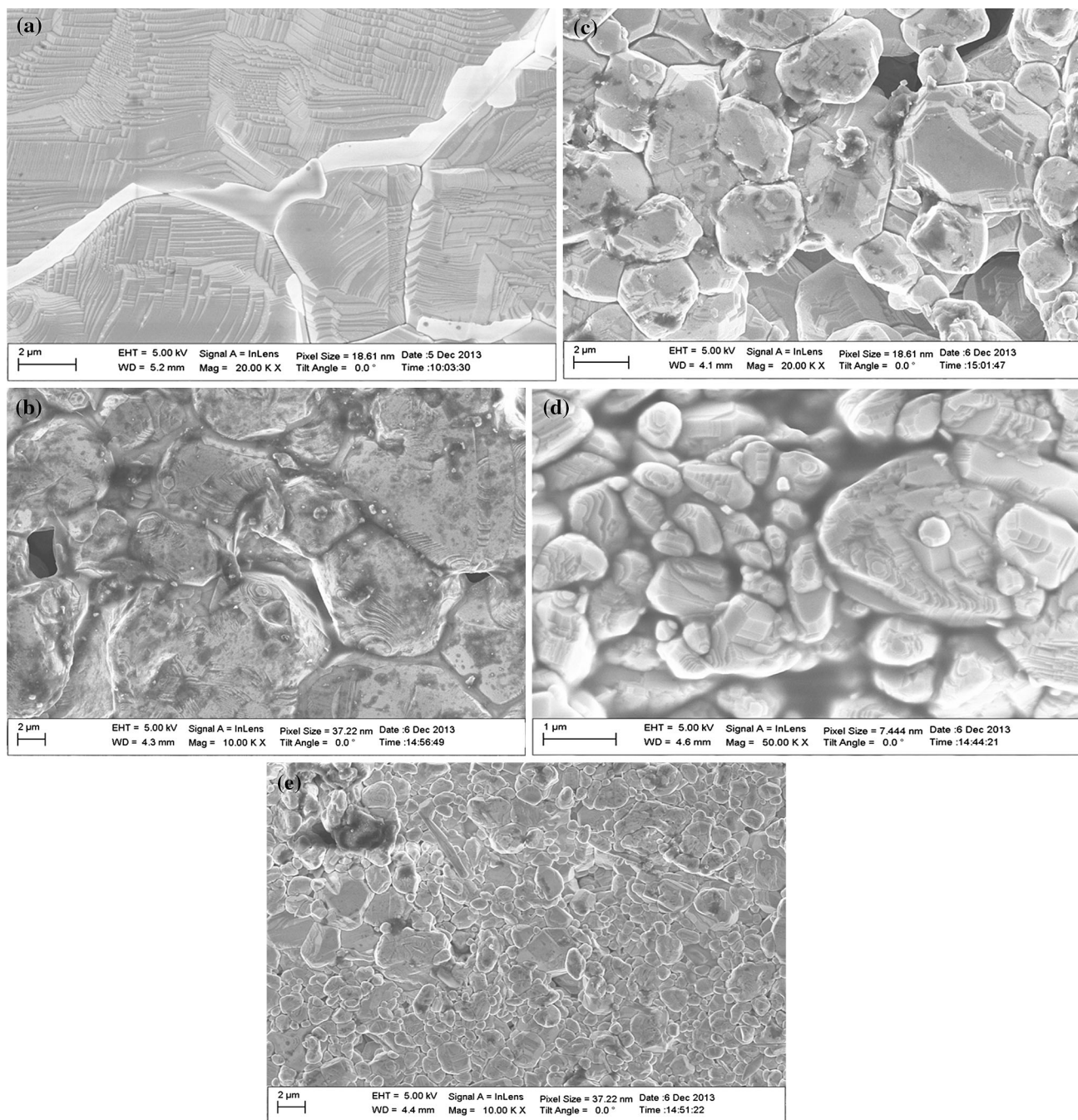


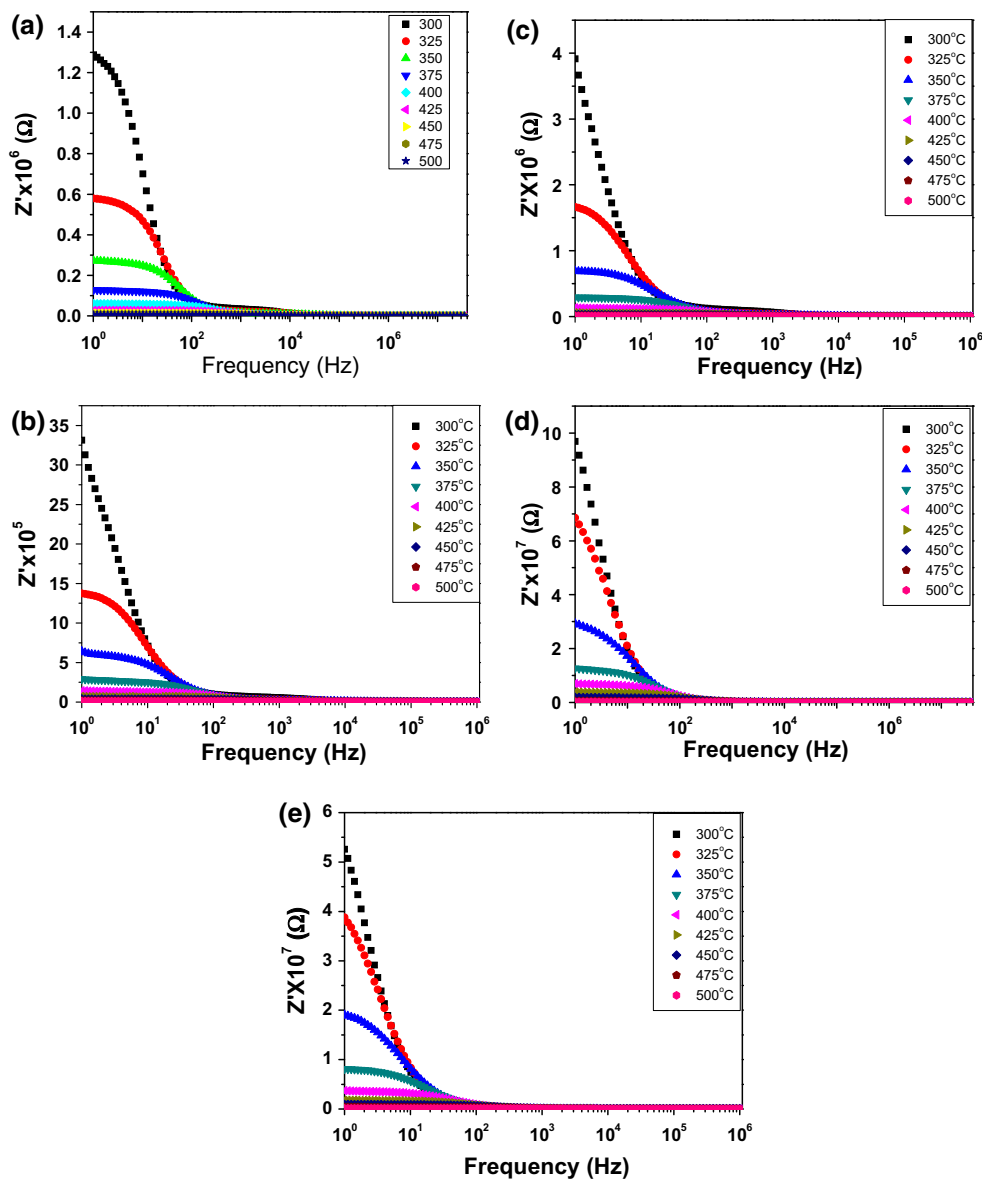
**Fig. 4** SEM micrograph of  $\text{Ba}_{1-x}\text{Sr}_x\text{Zr}_{0.05}\text{Ti}_{0.95}\text{O}_3$  ceramics, **a**  $x = 0.0$ , **b**  $x = 0.1$ , **c**  $x = 0.2$ , **d**  $x = 0.3$  and **e**  $x = 0.5$

### 3.2 SEM images analyses

Figure 4a–e illustrate SEM images of sintered BSZT ceramics. The nature of the microstructures of BSZT ceramics indicates that the grains were densely packed. SEM images showed the presence of large and small grains in microstructure for pure BZT ceramics and doped BSZT ceramics, respectively. Therefore, the incorporation of  $\text{Sr}^{2+}$  ions in A-site of the BZT lattice promotes a reduction in average grain size. All compositions show non-

uniformly distributed grains due to the characteristic of matter transport mechanism between the grains during the sintering process. At the initial stages of solid state reaction, the carbonates and oxides were ball milled in order to reduce the powder particle sizes. The heat promoted slow kinetics of inter-diffusion in the contact points between the particles with irregular morphologies. This diffusion resulted into irregularly shaped grains due to an elastic deformation caused by the surface energy reduction in the contact interface by its orientation and mobility.

**Fig. 5** Variations of real part  $Z'$  of  $Ba_{1-x}Sr_xZr_{0.05}Ti_{0.95}O_3$  ceramics with frequency at different temperatures  
**a**  $x = 0.0$ , **b**  $x = 0.1$ , **c**  $x = 0.2$ ,  
**d**  $x = 0.3$  and **e**  $x = 0.5$



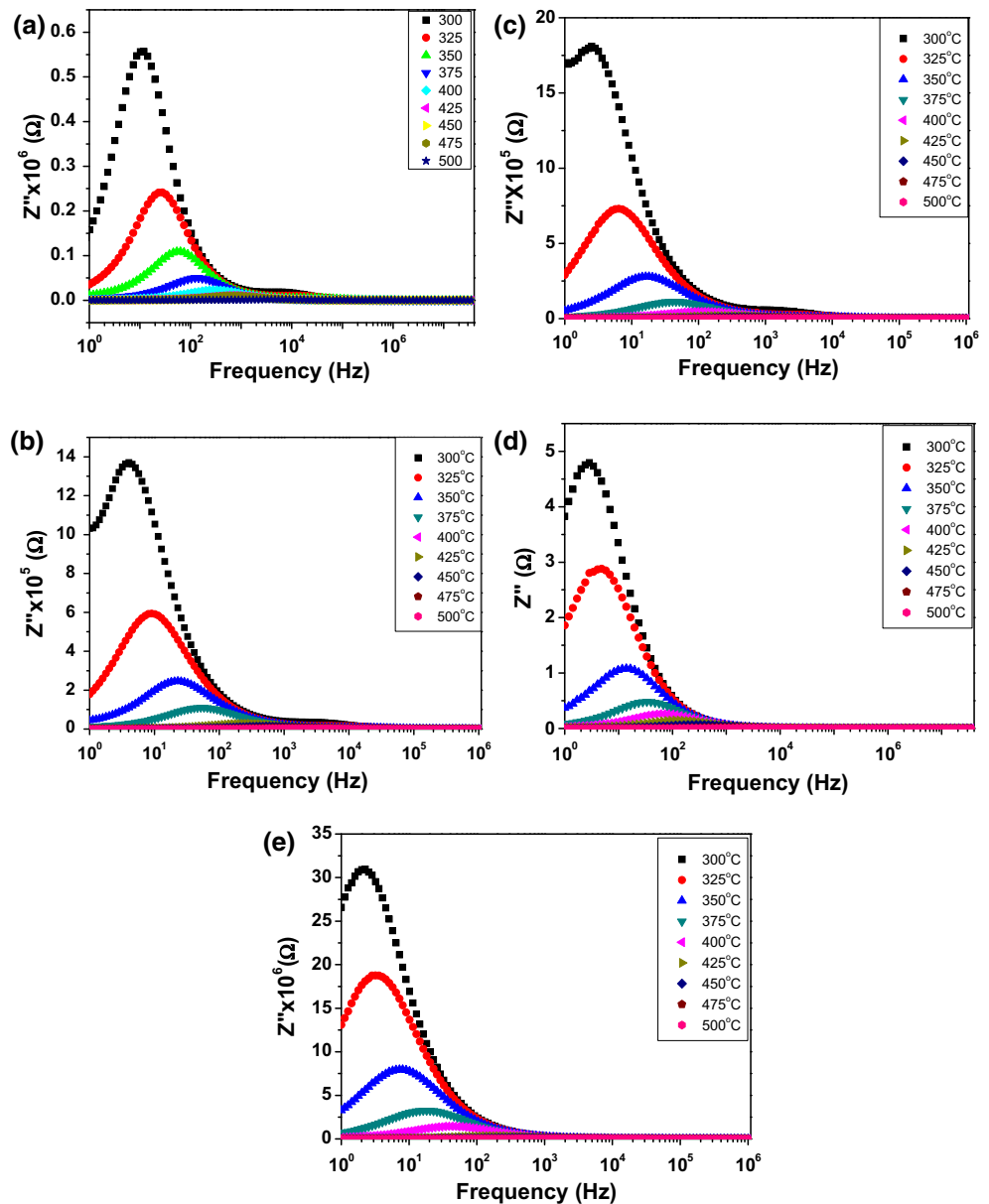
### 3.3 Impedance study

Figure 5a–e shows the variation of the real part of impedance ( $Z'$ ) as a function of frequency for all the samples. The nature of variation shows a monotonous decrease in the value of  $Z'$  with rise in the frequency. The impedance value is higher at lower temperatures in the low frequency region and decreases gradually with increase in frequency. The value of  $Z'$  also shows a decreasing trend with rise in temperature in the low frequency domain, but tends to merge with the low temperature data in the high-frequency region. The decrease in  $Z'$  with rise in temperature and frequency also indicates a possibility of increase in the conductivity with increase in temperature and frequency. The merger of real part of impedance ( $Z'$ ) in the high frequency domain for all temperatures indicates a

possibility of the release of space charge as a result of lowering in the barrier properties of the material. These results indicate that electrical conduction will increase with the rise in temperature and the phenomenon is dependent on release of space charge. It was also observed that the values were increasing as the Sr content increased. The increases in Sr content allowed more grain aggregates which increased the area of potential barrier between the grains and offered more resistance for charge carrier.

Figure 6a–e show the variation of the imaginary part of the impedance  $Z''$  with frequency at different temperatures for BSZT. The  $Z''$ -frequency patterns exhibited some important features such as (i) appearance of a peak at a particular frequency (known as relaxation frequency), (ii) decrease in the magnitude of  $Z''$  with a clear shift in the peak frequency toward higher frequency, and (iii) peak

**Fig. 6** Variations of imaginary part  $Z''$  of  $\text{Ba}_{1-x}\text{Sr}_x\text{Zr}_{0.05}\text{Ti}_{0.95}\text{O}_3$  ceramics with frequency at various temperatures **a**  $x = 0.0$ , **b**  $x = 0.1$ , **c**  $x = 0.2$ , **d**  $x = 0.3$  and **e**  $x = 0.5$



broadening with a rise in temperature. A significant broadening of the peaks with an increase in temperature suggests the existence of a temperature-dependent electrical relaxation phenomenon in the material. The asymmetric broadening of the peaks suggests the presence of electrical processes in the material with a spread of relaxation time. The effect of an increase in Sr substitution on the electrical behavior of the samples can clearly be seen in terms of (i) an increase in the magnitude of  $Z''$  (ii) shift in the peak frequency toward lower frequency, and (iii) peak broadening and asymmetry. The shifting of the peak frequency toward the lower frequency side with doping the Sr at Ba site indicates the increase in the relaxation time. As the concentration of Sr increases, the increase in the broadening

and asymmetry of the peaks suggests that there is an increase in the distribution of relaxation times and departure from ideal Debye-like behavior. The relaxation species in the material may be immobile species/electrons at low temperature and defects/vacancies at higher temperature. This result also shows the significant effect of Sr substitution on the electrical behavior of BZT.

Figure 7a–e shows the temperature dependence of complex impedance spectra (Nyquist plots) of BSZT. The impedance spectrum is characterized by the appearance of semicircular arcs whose radius decreases with increase in temperature. The complex impedance plots comprise two overlapping semicircular arcs with the center below the real axis. According to Debye's model, a material having a

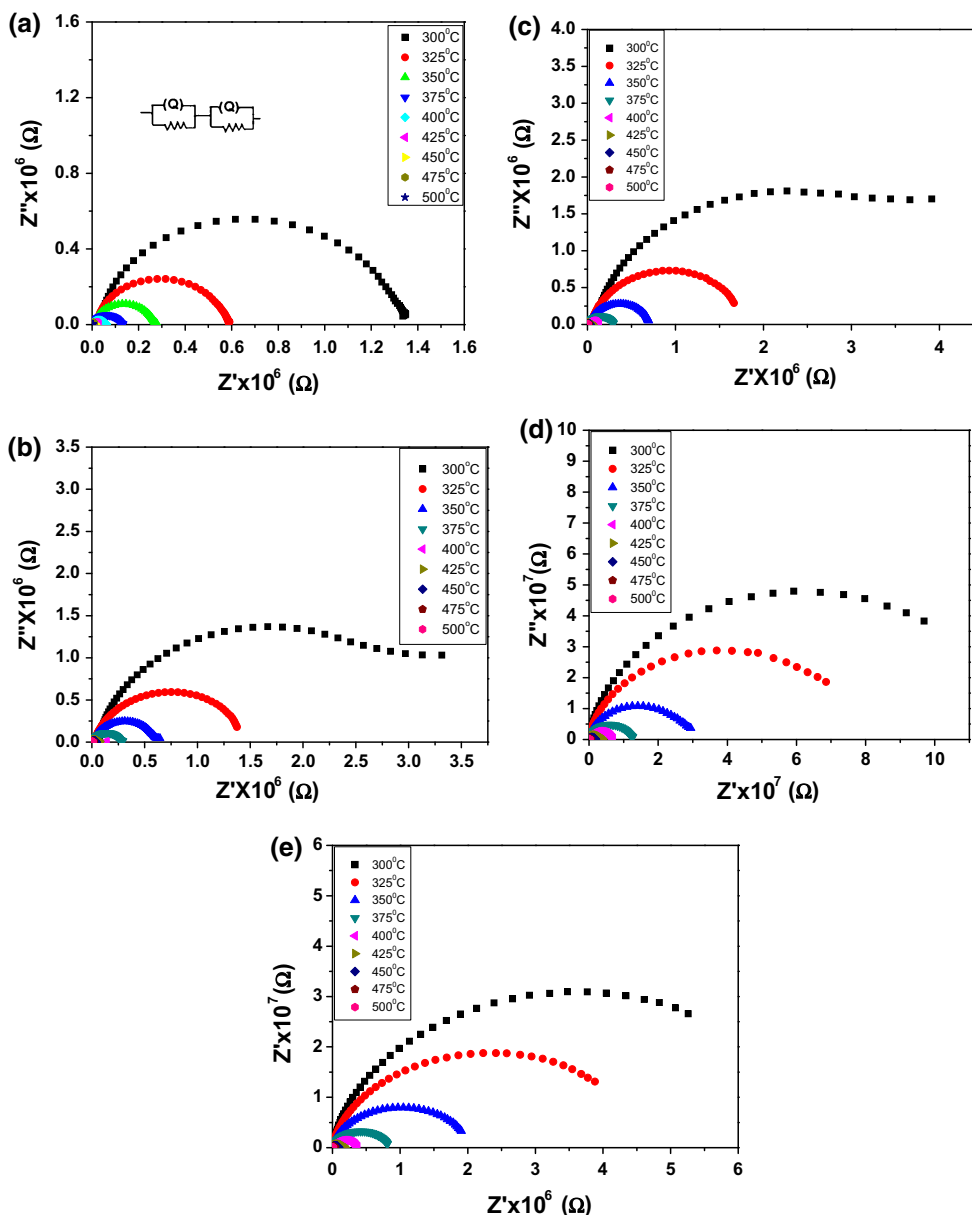


**Fig. 7** Cole–Cole plots between  $Z'$  and  $Z''$  for  $Ba_{1-x}Sr_xZr_{0.05}Ti_{0.95}O_3$  ceramics measured at various temperatures: **a**  $x = 0.0$ , **b**  $x = 0.1$ , **c**  $x = 0.2$ , **d**  $x = 0.3$  and **e**  $x = 0.5$

single relaxing time gives rise to an ideal semicircle centered on the real axis. The shape of our plots suggests that the electrical response is composed of at least two relaxation phenomena with different relaxation frequencies. The high frequency semicircle is due to the bulk property of the materials where the low frequency arc is due to the grain boundary in the materials.

For successful data analysis, an equivalent circuit model consisting of some combinations of resistance ( $R$ ) and capacitance ( $C$ ) elements connected in series and/or parallel is required to model the impedance data and represent physically the various charge migrations and polarization phenomena

occurring in the ceramics. The impedance data are fitted using two RQ circuit in series  $(R_{gb}Q_{gb})(R_gQ_g)$  (shown in inset of Fig. 7a) by the Zsimwin software, where,  $R_{gb}$ ,  $R_g$  and  $Q_{gb}$ ,  $Q_g$  are the resistances and constant phase elements of two electroactive regions, i.e., grain boundary, and grain, respectively. The term  $Q$  represents a non-ideal capacitance which is physically determined by parameter admittance ( $Y'$ ) with exponent  $n$  being  $n \leq 1$ . This departure exhibited by the parameter  $Q$  is exclusively due to the distribution of the relaxation times, which leads to the decentralization phenomenon of the semicircle [14–19]. The capacitance of  $Q$  is obtained from the expression,  $C = R^{(1-n)/n} Q^{1/n}$ , where the value of parameter  $n$

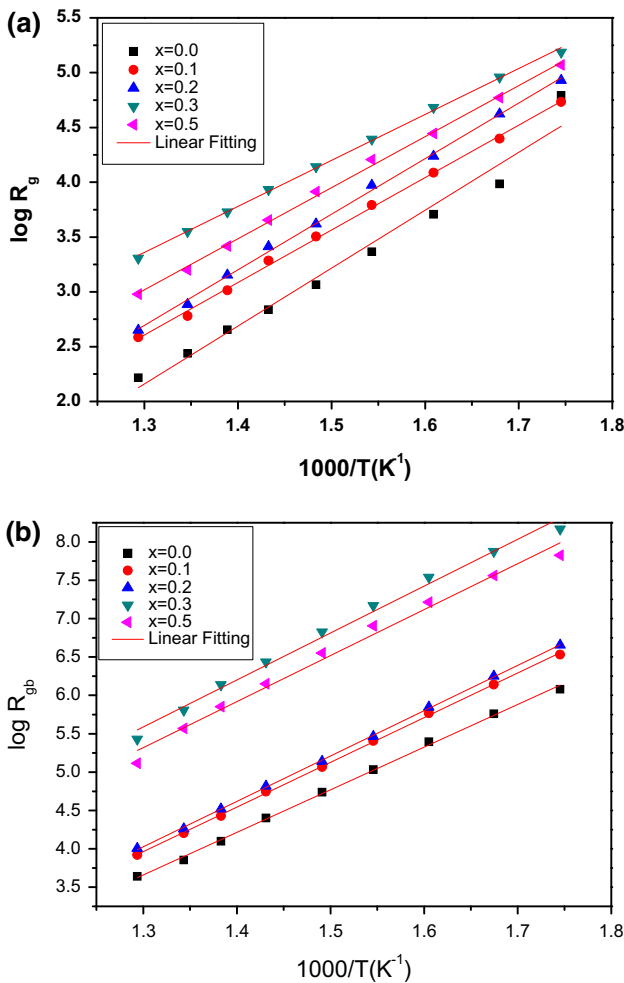


**Fig. 8** Arrhenius plot of resistance for the Ba<sub>1-x</sub>Sr<sub>x</sub>Zr<sub>0.05</sub>Ti<sub>0.95</sub>O<sub>3</sub> ceramics **a** Grain and **b** Grain boundary

**Table 1** Activation energy (in eV) calculated from different parameters of Ba<sub>1-x</sub>Sr<sub>x</sub>Zr<sub>0.05</sub>Ti<sub>0.95</sub>O<sub>3</sub> ceramics

Composition	Z''	M''	R <sub>g</sub>	R <sub>gb</sub>	σ <sub>dc</sub>
x = 0.0	0.52	0.46	0.45	0.47	0.48
x = 0.1	0.53	0.48	0.43	0.50	0.49
x = 0.2	0.56	0.50	0.41	0.51	0.52
x = 0.3	0.57	0.52	0.36	0.52	0.57
x = 0.5	0.54	0.47	0.40	0.51	0.50

lies between 0 and 1. If n = 1, the constant phase element will behave as a pure capacitor and for n = 0 it acts as a pure resistor. Constant phase element “Q” is used to accommodate the heterogeneity present in the sample. The values of the circuit elements obviously depend on the volume fraction of the individual components (i.e., grain and grain boundary effects), In ceramics, grain boundaries are often electronically active due to depletion effects and act as barriers to the cross

**Table 2** The thermistor parameter α and β for Ba<sub>1-x</sub>Sr<sub>x</sub>Zr<sub>0.05</sub>Ti<sub>0.95</sub>O<sub>3</sub> ceramic

Composition	α	β
x = 0.0	0.01685	4211.48537
x = 0.1	0.01759	4,396.7975
x = 0.2	0.01889	4,722.41621
x = 0.3	0.01823	4,558.71521
x = 0.5	0.01873	4,683.18664

transport of the charge carriers. The electrical phenomena can be expressed in terms of a bricklayer model, where the conduction through the grain and grain boundaries dominates. This fitting is based on the non-linear least square fitting where an algorithm is used for fitting.

It is observed from the fitting data that at all temperatures, R<sub>b</sub> < R<sub>gb</sub>. The resistance associated with grain and grain boundary obeys the Arrhenius equation as,

$$R = R_0 \exp \frac{E_a}{K_B T} \tag{1}$$

The activation energy is calculated from Arrhenius plot as shown in Fig. 8a,b and presented in Table 1. The Ea for grain boundaries is found to be higher than that of grains indicating higher resistive behavior than that of grains. The values obtained for E<sub>g</sub> and E<sub>gb</sub> suggest that relaxation peak at lower frequency could be due to oxygen vacancies at grain boundaries (and/or possibly domain boundaries) whereas peak at high frequency is due to the oxygen vacancy related defects relaxation inside the grain [20]. In crystalline materials, the surface atoms on the grains will have a higher diffusion coefficient than that of the lattice grains and thus the grain boundary is expected to have a higher conductivity [21]. The activation energy of the grain boundary is a little higher than that of the grain. The value of the activation energy for conduction clearly suggests a possibility that the conduction in the higher temperature range for ionic charge carriers may be oxygen vacancies. In perovskite ferroelectric materials oxygen vacancies are considered as one of the mobile charge carriers [22] and mostly in titanates, ionization of oxygen vacancies creates conduction electrons, a process which is defined by the Kroger-Vink notation as [23]



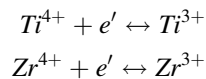
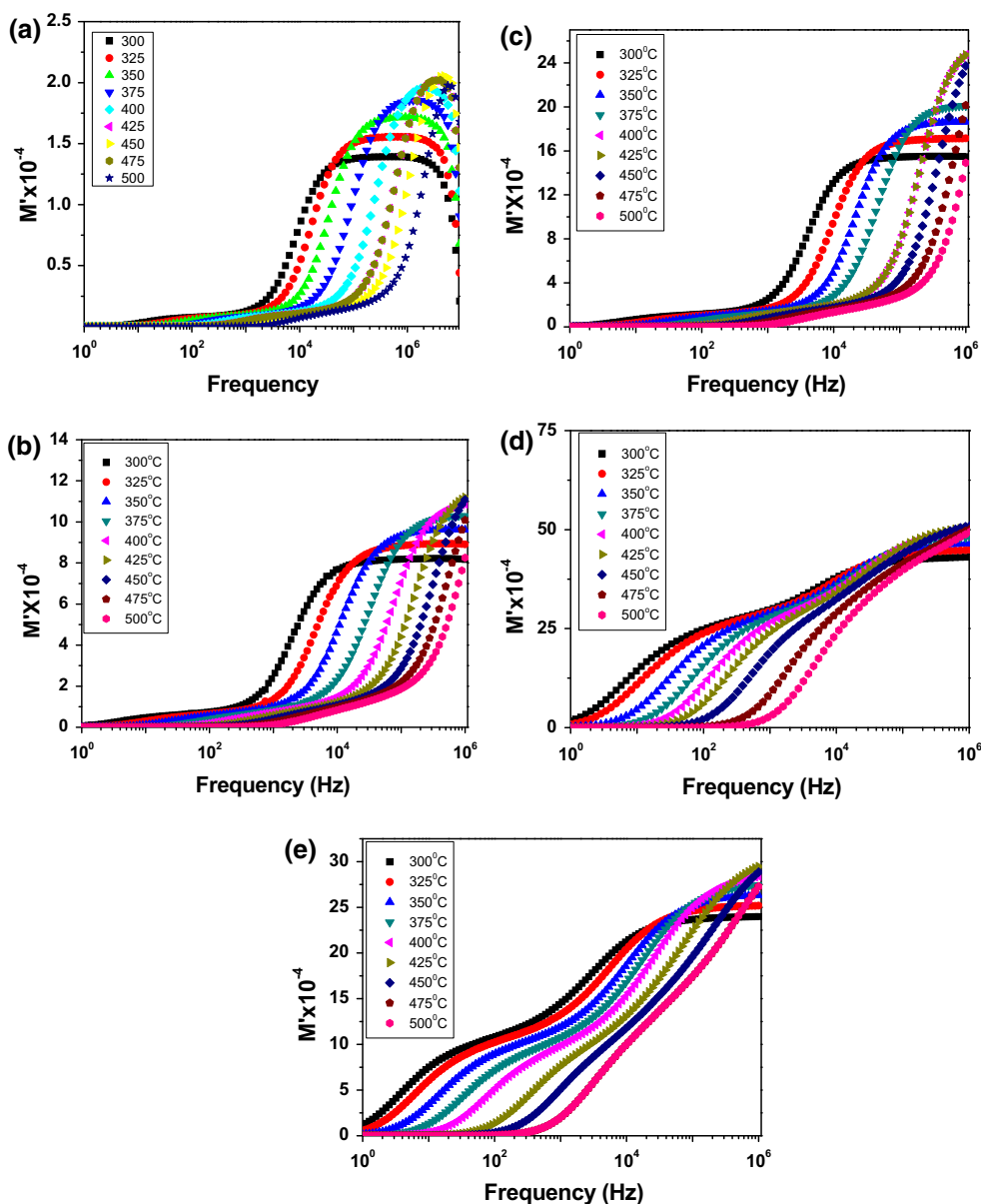
Thus, excess electrons and oxygen vacancies are formed in the reduction reaction



And they may bond to Ti<sup>4+</sup> and Zr<sup>4+</sup> in the form



**Fig. 9** Variations of a real part of  $M'$  for  $Ba_{1-x}Sr_xZr_{0.05}Ti_{0.95}O_3$  ceramics with frequency at different temperatures: **a**  $x = 0.0$ , **b**  $x = 0.1$ , **c**  $x = 0.2$ , **d**  $x = 0.3$  and **e**  $x = 0.5$



$$(4) \quad R_T = R_N \exp \left[ \beta \left( \frac{T_N - T}{TT_N} \right) \right], \tag{5}$$

These electrons trapped by  $Ti^{3+}$  or  $Zr^{3+}$  ions or oxygen vacancies can be thermally activated, thus enhancing the conduction process. Doubly charged oxygen vacancies are considered to be the most mobile charges in perovskite ferroelectrics and play an important role in conduction [24].

where  $R_T$  is the resistance at temperature  $T$ ,  $R_N$  the resistance at temperature  $T_N$  is known, and  $\beta$  is an NTC thermistor characteristic parameter.

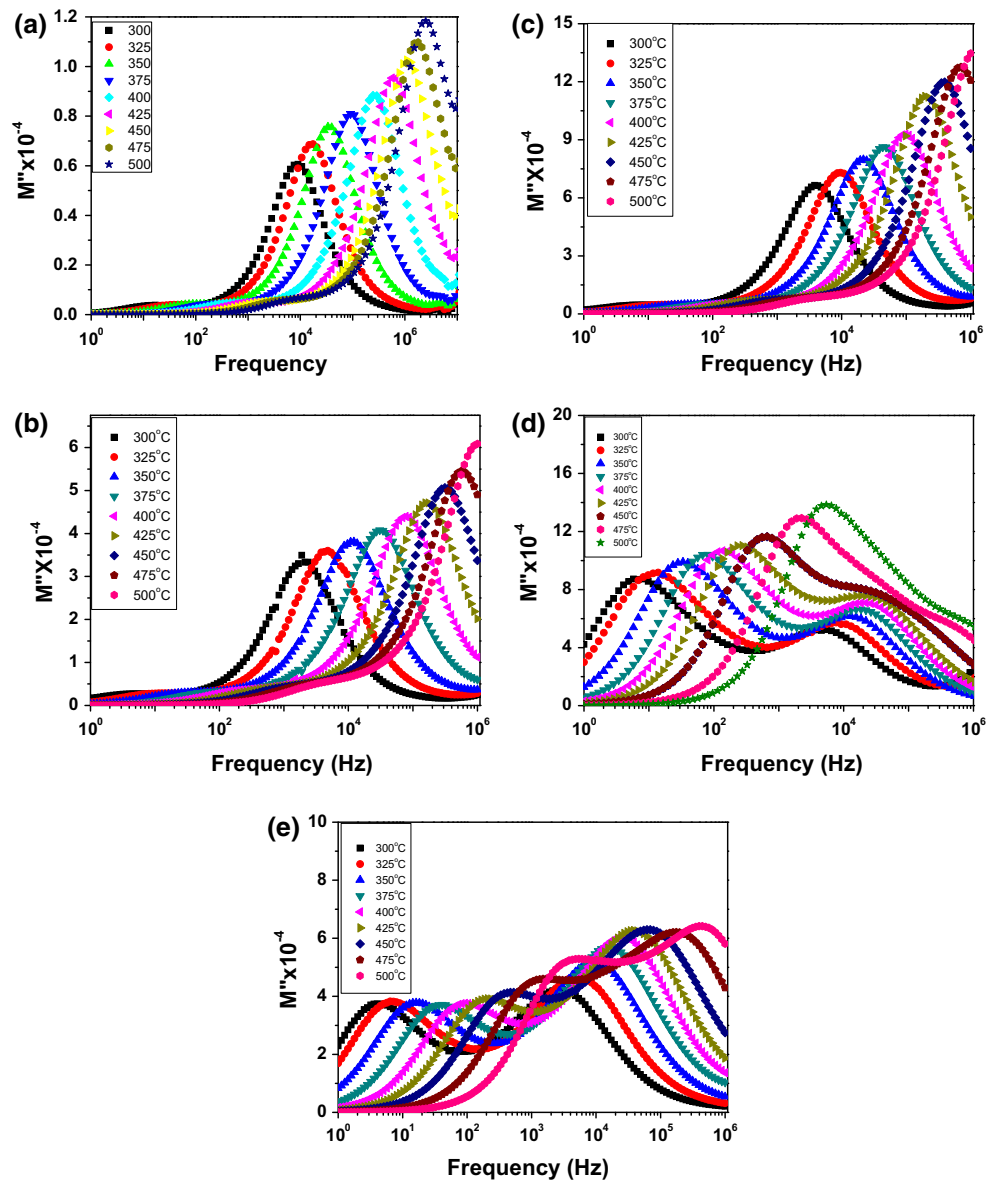
It is observed from the impedance analysis that the resistance of the materials decreases with increase in temperature resulting NTCR behavior in the materials. The relation between resistance and temperature for a compound exhibiting NTCR behavior is expressed as,

The thermistor characteristic parameter can be expressed as

$$\beta = \left[ \frac{TT_N}{T_N - T} \right] \ln \frac{R_T}{R_N} \tag{6}$$

The sensitivity of the thermistor  $\beta$  can be also defined by the temperature coefficient of resistance ( $\alpha$ ), which can be

**Fig. 10** Variations of imaginary part of  $M''$  for  $\text{Ba}_{1-x}\text{Sr}_x\text{Zr}_{0.05}\text{Ti}_{0.95}\text{O}_3$  ceramics with frequency at different temperatures: **a**  $x = 0.0$ , **b**  $x = 0.1$ , **c**  $x = 0.2$ , **d**  $x = 0.3$  and **e**  $x = 0.5$



expressed as a function of  $\beta$  parameter according to the following equation

$$\alpha = \left(\frac{1}{R}\right) \left[\frac{d(R)}{dT}\right] = -\frac{\beta}{T^2} \quad (7)$$

The various thermistor parameters are given in Table 2. Thus, the high value of  $\beta$  obtained endorsed BSZT as a good quality NTC material for the fabrication of thermistor devices.

### 3.4 Modulus spectroscopy analyses

The frequency and temperature dependence of the real part of the modulus ( $M'$ ) of BSZT with  $x = 0.00, 0.1, 0.2, 0.3$  and  $0.5$  is shown in Fig. 9a–e.  $M'$  approaches to zero at all temperatures, suggesting the suppression of electrode polarization.  $M'$  reaches a maximum value corresponding to  $M_\infty$  due

to the relaxation process. It is also observed that the value of  $M_\infty$  decreases with increase in temperature. These graphs show that modulus peaks shift towards the high frequency side on increasing temperature.  $M'(\omega)$  shows a dispersion tending toward  $M_\infty$  (the asymptotic value of  $M'(\omega)$  at higher frequencies). The nature of variation indicates that the electrical properties of the material arise due to the bulk (intra-grain) property. In the low temperature region, the value of  $M'$  increases with the increase in frequency and decreases with rise in temperature with slow rate. While in the high-temperature region, the value of  $M'$  increases rapidly with an increase in both the temperature and frequency. It may be contributing to conduction phenomena due to the short range mobility of charge carriers. This implies the lack of a restoring force for flow of charge under the influence of a steady electric field [25].

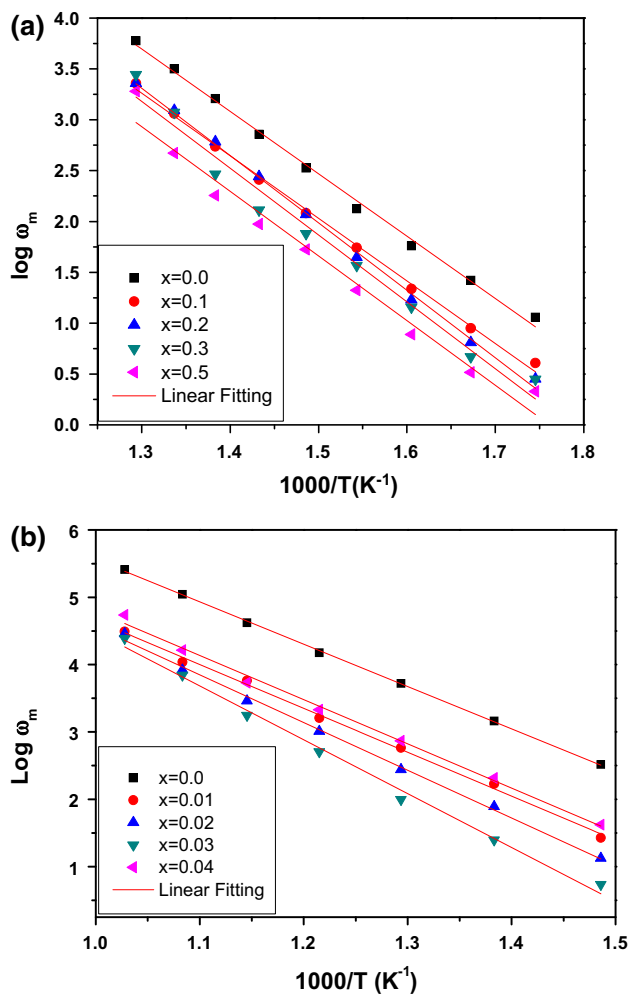


**Fig. 11** Arrhenius plot of  $\log \omega_{max}$  from imaginary part of **a** impedance and **b** modulus

The frequency and temperature dependence of the imaginary part of the modulus ( $M''$ ) of BSZT with  $x = 0.00, 0.1, 0.2, 0.3$  and  $0.5$  is shown in the Fig. 10a–e. Two characteristic peaks were observed in all compositions representation both grain and grain boundary effect. The frequency region below the peak frequency of  $M''$  versus frequency spectra determines the range in which charge carriers are mobile over long distances. The asymmetric modulus peaks shift towards the high frequency side with a rise in temperature exhibiting the correlation between the motions of mobile charge carriers [26]. The observed  $M''$  peaks of the plots are related to conductivity relaxation of the materials. The asymmetry in peak broadening shows the spread of relaxation times with different time constant, and hence the relaxations of non-Debye type. The existence of low frequency peaks suggests that the ions can move over long distances where as high frequency peaks suggest about the confinement of ions in their potential well. The nature of modulus spectra confirms the existence of

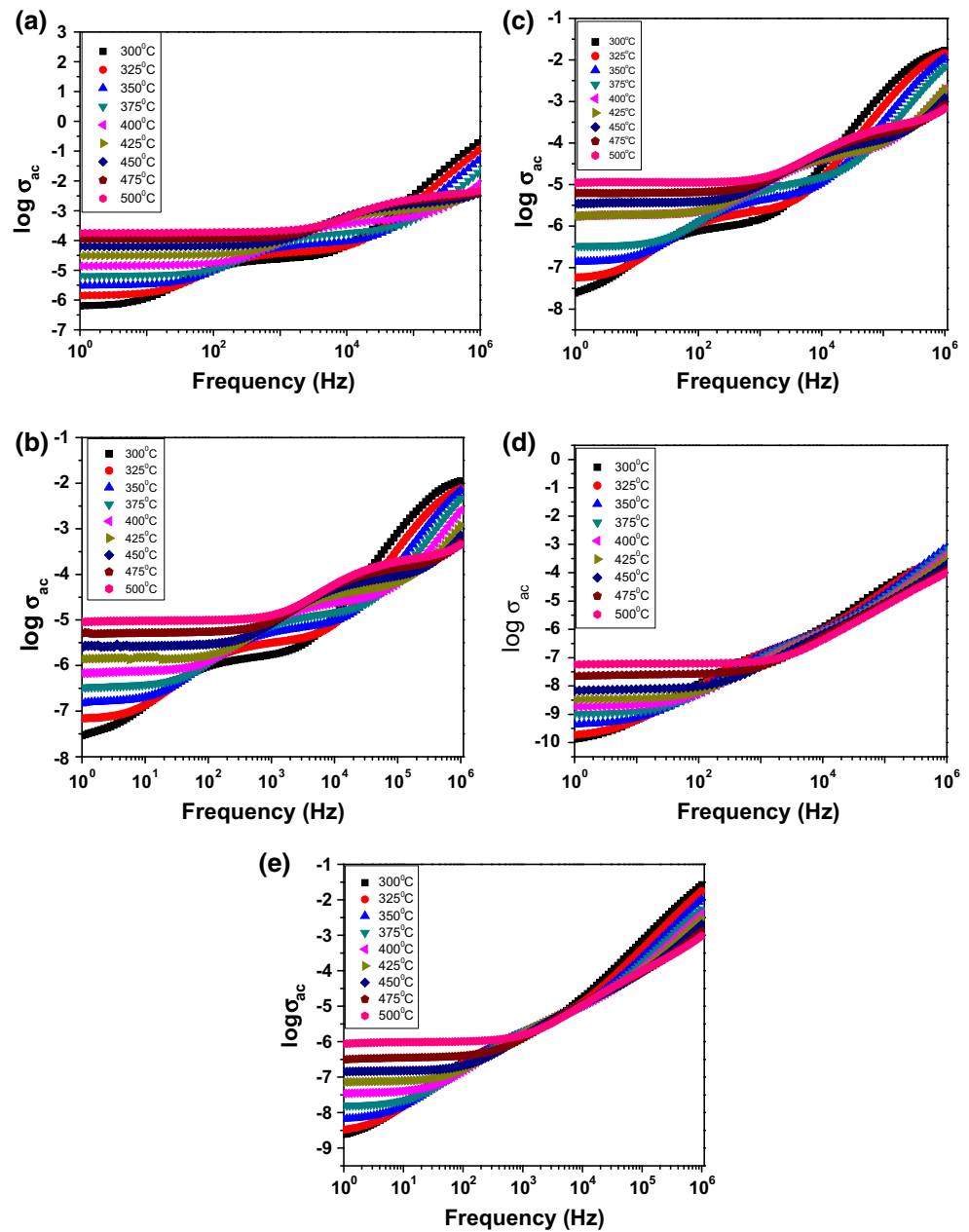
hopping mechanism in the electrical conduction of the materials. From the figures, it can be observed that the deviations of maximum peak frequencies are increasing with increase in the concentration of  $Sr^{2+}$  ions in the BZT system. Therefore, the doped samples show the short range movement of charge carriers and the un-doped sample shows the long range movement of charge carriers. A non-exponential type of conductivity relaxation suggests that ion migration takes place via hopping accompanied by a consequential time dependent mobility of other charge carriers of the same type in the vicinity [19]. For  $x = 0.0$ , a broad single peak is observed in  $M''$  spectra whose position appears to be shifting toward higher frequencies at increasing temperatures. It has been observed that the height and broadening of the modulus peak appear to decrease with an increase in Sr concentration. The decrease in the modulus peak height on increasing  $x$  suggests an enhancement in the capacitance value of the sample on substitution of Sr in the compound [27].

Figure 11a,b shows the variation of relaxation time  $\omega_m$  calculated from  $Z''$  and  $M''$  versus frequency plot respectively with reciprocal of temperature i.e.,  $\log \omega_m$  versus  $10^3/T (K)$  for different Sr concentration, which follows the Arrhenius behavior. The calculated activation energy is given in Table 1. It is interesting to note that the activation energy obtained from the  $Z''$  spectra represents the localized conduction (i.e., dielectric relaxation) whereas the activation energy obtained from the  $M''$  spectra represents non-localized conduction (i.e., long-range conduction) [28]. From the figure, it has been observed that the relaxation times decrease with an increase in Sr concentration. Again, the activation energy of the localized conduction (i.e., dielectric relaxation) and non-localized conduction (i.e., long-range conduction) decreases with an increase in Sr concentration systematically. The activation energy for  $x = 0$  is found to be nearly 0.5 eV from the relaxation time obtained from the  $M''$  and  $Z''$  versus frequency plot. This range of activation energy is typical for oxygen vacancies or  $3d$ -metal–oxygen vacancies in various perovskite materials.

### 3.5 Ac conductivity

The variation of Ac conductivity with different frequencies at different temperatures for all the compounds is shown in Fig. 12a–e. The power law dependence of Ac conductivity is of a universal nature and corresponds to a short range hopping of charge carriers through trap sites separated by energy barriers of varied heights. Each pair of potential well corresponds to a certain time constant of transition from one site to another. The conductivity  $\sigma_{ac}$  can be written as  $\sigma_{ac} = \sigma_{dc} + A\omega^n$  known as Jonscher’s power law [29] where  $n$  is the frequency exponent in the range of

**Fig. 12** The frequency dependence of the ac conductivity for  $\text{Ba}_{1-x}\text{Sr}_x\text{Zr}_{0.05}\text{Ti}_{0.95}\text{O}_3$  ceramics with frequency at various temperatures: **a**  $x = 0.0$ , **b**  $x = 0.1$ , **c**  $x = 0.2$ , **d**  $x = 0.3$  and **e**  $x = 0.5$



$0 < n < 1$ . According to Jonscher, the origin of frequency dependence of conductivity lies in the relaxation phenomena arising due to mobile charge carriers. The low frequency dispersion is attributed to the Ac conductivity whereas the frequency independent plateau region in the conductivity pattern corresponds to the d.c. conductivity of the material sample. The frequency at which the slope change takes place is known as the hopping frequency, which corresponds to polaron hopping of charged species [30]. The hopping frequency shifts to the higher frequency side with temperature.

The above-mentioned observation in conductivity spectra can be explained on the basis of the jump relaxation model and conduction through grain boundaries. The frequency independent plateau at a low frequency is attributed to the long-range translational motion of ions contributing to dc conductivity ( $\sigma_{dc}$ ). The observed frequency independent dc conductivity was explained by Funke [30] in the jump relaxation model (JRM). According to this model, the conductivity at the low frequency region is associated with the successful hops to its neighboring vacant site due to the available long time period; such successive jumps

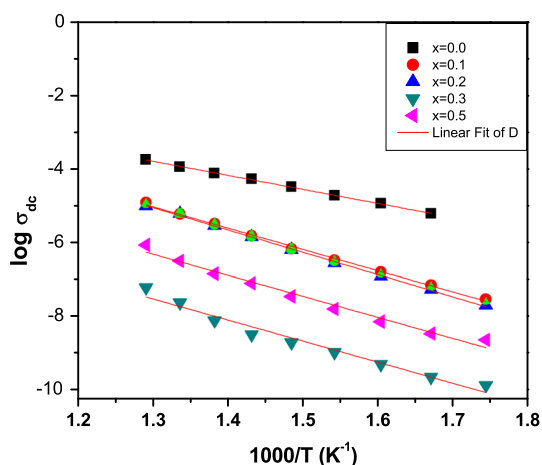


**Fig. 13** Temperature dependence of the dc conductivity curve for the BSZT ceramic. The *dots* are the experimental points and the *solid line* is the least-square *straight line* fit

result in a long-range translational motion of ions contributing to dc conductivity. The dc conductivity was calculated from the frequency independent part and the variation of dc conductivity with temperature is shown in Fig. 13. The conductivity variation indicates an increase in conductivity with rise in temperature with a typical Arrhenius-type behaviour. The type of temperature dependence of Dc conductivity indicates that the electrical conduction in the material is a thermally activated process. The activation energy was calculated from the linear portion of the plot of Dc conductivity ( $\sigma$ ) versus  $10^3/T$  (Fig. 13). In ceramic samples, oxygen vacancies are usually considered as one of the mobile charge carriers in ferroelectric perovskite. The ionization of oxygen vacancies creates conducting electrons, which are easily thermally activated. From the results of conduction and the value of the activation energy for conduction, it clearly suggests a possibility that the conduction in the higher-temperature range for charge carriers may be oxygen vacancies [31].

#### 4 Conclusion

The present work reports the structural and electrical properties of BSZT compounds prepared through High energy ball milling. The X-ray diffraction study shows a single phase in all compounds and the structure changes from tetragonal to cubic at  $x \geq 0.3$ . Complex impedance spectroscopy, in terms of a simultaneous analysis of the complex impedance, is used to investigate the electrical behaviour of the ceramics. The complex impedance spectroscopy indicates the possible contributions of the bulk and grain boundaries and also temperature-dependent relaxation. Modulus analysis establishes the possibility of

hopping mechanism for electrical transport processes in the system. Almost the same activation energies calculated from relaxation time of impedance and modulus plots indicate the existence of both types of charge carriers. The compounds exhibit negative temperature coefficient of resistance (NTC) behavior and temperature dependent relaxation phenomena. The Ac conductivity follows the universal power law. The activation energy calculated for both bulk and grain boundary effect suggests the possibility of electrical conduction due to the mobility of oxide ions or oxide ion vacancies at higher temperature.

#### References

1. G. Goodman, *Ceramic capacitor materials, in Ceramic Materials for Electronics* (Marcel Dekker, New York, 1986)
2. L.L. Hench, L.K. West principles of electronic ceramics. New York: John Wiley & Sons. Inc. (1990)
3. T.G. Reynolds, Application space influences electronic ceramic materials. *Am. Ceram. Soc. Bull.* **80**, 29–32 (2001)
4. Y. Park, Y.H. Kim, H.G. Kim, The effect of grain size on dielectric behavior of BaTiO<sub>3</sub>-based X7R materials. *Mater. Lett.* **28**, 101–106 (1996)
5. F. Azough, R. Al, Saffar, R. Freer, A transmission electron microscope study of commercial X7R-type multilayer ceramic capacitors. *J. Eur. Ceram. Soc.* **18**, 751–758 (1998)
6. H. Kishi, Y. Mizuno, H. Chazono, Base-metal Electrode multilayer ceramic capacitors: past, present and future perspectives. *Jpn. J. Appl. Phys.* **42**, 1–15 (2003)
7. R.Z. Chen, A.L. Cui, X.H. Wang, L. Li, Barium titanate coated with magnesium titanate via fused salt method and its dielectric property. *Mater. Sci. Eng., B* **99**, 302–305 (2003)
8. J.F. Chen, Z.G. Shen, F.T. Liu, X.L. Liu, J. Yun, Preparation and properties of barium titanate nanopowder by conventional and high-gravity reactive precipitation methods. *Scr. Mater.* **49**, 509–514 (2003)
9. K. Uchino, *Ferroelectric devices, ferroelectric devices* (Marcel Dekker, New York, 2000)
10. S.K. Jo, S.H. Kang, Y.H. Han, Redox behavior and electrical properties of Sr and Zr substituted BaTiO<sub>3</sub>. *J. Electroceram.* **31**, 189–193 (2013)
11. R.D. Levi, Ph.D. Thesis, Penn State University (2009)
12. J.A. Basmajian, R.S. De Vries, Phase Equilibria in the System BaTiO<sub>3</sub>-SrTiO<sub>3</sub>. *J. Am. Ceram. Soc.* **40**, 373–376 (1957)
13. J. Bera, S.K. Rout, On the formation mechanism of BaTiO<sub>3</sub>-BaZrO<sub>3</sub> solid solution through solid-oxide reaction. *Mater. Lett.* **59**, 135–138 (2005)
14. L.E. Cross, Relaxor Ferroelectrics. *Ferroelectrics* **76**, 241–247 (1987)
15. S. Nomura, Dielectric properties of titanates containing Sn<sup>4+</sup> Ions I. *J. Phys. Soc. Jpn.* **10**, 112–119 (1955)
16. G.A. Smolensky, V.A. Isupov, A.I. Agranovskaya, A new group of ferroelectrics (with layered structure)". *Soviet Physics Solid State* **1**, 149–150 (1959)
17. M.A.L. Nobre, S. Lanfredi, Dielectric properties of Bi<sub>3</sub>Zn<sub>2</sub>Sb<sub>3</sub>O<sub>14</sub> ceramics at high temperature. *Mater. Lett.* **47**, 362–366 (2001)
18. S. Sen, R.N.P. Choudhary, Dielectric relaxation in Sr modified PST ceramics. *Appl. Phys. A* **87**, 727–731 (2007)
19. J.R. Macdonald, *Impedance Spectroscopy: Emphasizing Solid State Material and Systems* (Wiley, New York, 1987)

20. S. Kumar, K.B.R. Varma, Dielectric relaxation in bismuth layer-structured  $\text{BaBi}_4\text{Ti}_4\text{O}_{15}$  ferroelectric ceramics. *Curr. Appl. Phys.* **11**, 203–210 (2011)
21. P. Thangadurai, V. Sabarinathan, A.C. Bose, S. Ramasamy, Conductivity behaviour of a cubic/tetragonal phase stabilized nanocrystalline  $\text{La}_2\text{O}_3\text{-ZrO}_2$ . *J. Phys. Chem. Solids* **65**, 1905–1912 (2004)
22. T. Kimura, M. Machida, T. Yamaguchi, R.E. Newnham, Products of Reaction Between PbO and  $\text{Nb}_2\text{O}_5$ , in Molten KCl and NaClJ. *Am. Ceram Soc.* **66**, 195–197 (1983)
23. C. Ang, Z. Yu, Z. Jing, P. Lunkenheimer, A. Loidl, Dielectric spectra and electrical conduction in Fe-doped  $\text{SrTiO}_3$ . *Phys. Rev. B* **61**, 3922 (2000)
24. S. Sen, R.N.P. Choudhary, A. Tarafdar, P. Pramanik, Impedance spectroscopy study of strontium modified lead zirconate titanate ceramics. *J. Appl. Phys.* **99**, 124114 (2006)
25. P.B. Macedo, C.T. Moynihan, R. Bose, The role of ionic diffusion in polarization in vitreous ionic conductors. *Phys. Chem. Glasses* **13**, 171–179 (1972)
26. N. Ortega, A. Kumar, P. Bhattacharaya, S.B. Majumder, R.S. Katiyar, Impedance spectroscopy of multiferroic  $\text{PbZr}_x\text{Ti}_{1-x}\text{O}_3/\text{CoFe}_2\text{O}_4$  layered thin film. *Phys. Rev. B* **77**, 014111–014120 (2008)
27. D.K. Pradhan, R.N.P. Choudhary, C. Rinaldi, R.S. Katiyar, Effect of Mn substitution on electrical and magnetic properties of  $\text{Bi}_{0.9}\text{La}_{0.1}\text{FeO}_3$ . *J. Appl. Phys.* **106**, 024102–024104 (2009)
28. O. Raymond, R. Font, N. Suárez-Almodovar, J. Portelles, J.M. Siqueiros, Frequency-temperature response of ferroelectromagnetic  $\text{Pb}(\text{Fe}_{0.5}\text{Nb}_{0.5})\text{O}_3$  ceramics obtained by different precursors. Part II. Impedance Spectroscopy Characterization. *J. Appl. Phys.* **97**, 084108–084115 (2005)
29. A.K. Jonscher, *Dielectric Relaxation in Solids* (Chelsea Dielectric Press, London, 1983)
30. K. Funke, Jump relaxation in solid electrolytes. *Prog. Solid State Chem.* **22**, 111–195 (1993)
31. J.S. Kim, I.W. Kim, C.W. Ahn, T.K. Song, S.S. Kim, S.X. Chi, J.S. Bae, J.H. Jeong, Conduction behavior of  $\text{SrBi}_2\text{Ta}_2\text{O}_9$  thin film grown by pulsed laser deposition. *Jpn. J. Appl. Phys.* **41**, 6785–6789 (2002)